Accepted Manuscript

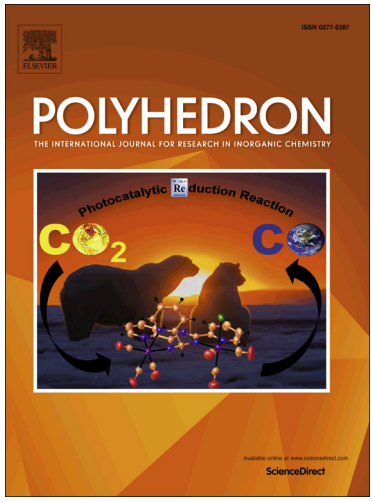

Experimental and theoretical investigation of octahedral and square-planar isothiocyanato complexes of Ni(II) with acylhydrazones of 2-(diphenylphosphino)benzaldehyde

Božidar Čobeljić, Andrej Pevec, Stepan Stepanović, Vojislav Spasojević, Milica Milenković, Iztok Turel, Marcel Swart, Maja Gruden-Pavlović, Kawther Adaila, Katarina Anđelković

PII: S0277-5387(15)00049-2
DOI: http://dx.doi.org/10.1016/j.poly.2015.01.024
Reference: POLY 11162

To appear in: *Polyhedron*

Received Date: 12 December 2014
Accepted Date: 23 January 2015

Please cite this article as: B. Čobeljić, A. Pevec, S. Stepanović, V. Spasojević, M. Milenković, I. Turel, M. Swart, M. Gruden-Pavlović, K. Adaila, K. Anđelković, Experimental and theoretical investigation of octahedral and square-planar isothiocyanato complexes of Ni(II) with acylhydrazones of 2-(diphenylphosphino)benzaldehyde, *Polyhedron* (2015), doi: http://dx.doi.org/10.1016/j.poly.2015.01.024

Experimental and theoretical investigation of octahedral and square-planar isothiocyanato complexes of Ni(II) with acylhydrazones of 2-(diphenylphosphino)benzaldehyde

Božidar Čobeljić[a], Andrej Pevec[b], Stepan Stepanović[c], Vojislav Spasojević[d], Milica Milenković[a], Iztok Turel[b], Marcel Swart[e,f], Maja Gruden-Pavlović[a], Kawther Adaila[a] and Katarina Anđelković[a*]

[a]*Faculty of Chemistry, University of Belgrade, Studentski trg 12-16, Belgrade, Serbia*

[b]*Faculty of Chemistry and Chemical Technology, University of Ljubljana, Večna pot 113, 1000 Ljubljana, Slovenia*

[c]*Center for Chemistry, IHTM, University of Belgrade, Studentski trg 12-16, Belgrade, Serbia*

[d]*Institute of Nuclear Sciences 'Vinča, Condensed Matter Physics Laboratory, P.O. Box 522, 11001 Belgrade, Serbia*

[e]*Institut de Química Computacional i Catàlisi (IQCC) and Departament de Química, Universitat de Girona, Campus Montilivi, Facultat de Ciències, 17071 Girona, Spain*

[f]*Institució Catalana de Recerca i Estudis Avançats (ICREA), Pg. Lluís Companys 23, 08010 Barcelona, Spain*

Keywords: Hydrazones; Ni(II) complex; PNO ligands; DFT calculations; X-ray structure.

Abstract

Octahedral and square-planar isothiocyanato complexes of Ni(II) with the condensation derivative of 2-(diphenylphosphino)benzaldehyde and Girard's T reagent were synthesized and characterized by elemental analysis, IR spectroscopy and X-ray crystallography. Results of magnetic measurements for octahedral Ni(II) complex were also reported. In all the complexes

* Corresponding author. Tel.: +381 11 3336739; fax: +381 11 3282 750.
e-mail address: kka@chem.bg.ac.rs

the ligand is coordinated as tridentate via the phosphorus, the imine nitrogen and the carbonyl oxygen atoms while the remaining coordination positions are occupied with thiocyanato anions. Coordination of deprotonated phosphine ligand results in formation of square-planar complexes, while the octahedral complex was formed with protonated ligand. Reaction energetics with both forms of ligand were studied by the means of DFT and results were in complete agreement with experimental observations. Furthermore, ligand field splitting analysis gave the deeper insight in the relationship of the isolated complex coordination environment and protonation of the ligand.

1. Introduction

Acylhydrazones of 2-(diphenylphosphino)benzaldehyde with "soft" phosphorus and "hard" nitrogen and oxygen donor atoms are potentially tridentate ligands that can exhibit a diversity of coordination modes. Depending on the central metal ion and reaction conditions acylhydrazones of 2-(diphenylphosphino)benzaldehyde can be either PNO tridentate, PN bidentate or P monodentate when protonated, and PNO tridentate when the ligand loses the hydrazonic proton [1–7]. Complexes of Ni(II) with acylhydrazones of 2-(diphenylphosphino)benzaldehyde are intensively investigated because of their interesting structural properties and biological activity [2–6]. In square-planar complexes of Ni(II) with 2-(diphenylphosphino)benzaldehyde benzoylhydrazone the ligand is coordinated in a monoanionic form through the PNO donor set while monodentate ligands (CH_3COO^-, Cl^-, $C{\equiv}C{-}C_6H_5^-$, $C{\equiv}C{-}t\mathrm{Bu}^-$) occupy the fourth coordination place [2]. Likewise, a square-planar environment around Ni(II) in the complex with the condensation derivative of 2-(diphenylphosphino)benzaldehyde and semicarbazide is formed by the tridentate PNO coordination of the monoanionic form of the ligand and an azide anion [3]. There is only one reported complex of Ni(II) with acylhydrazone of 2-(diphenylphosphino)benzaldehyde that adopts a tetrahedral coordination geometry. In this complex the condensation derivative of 2-(diphenylphosphino)benzaldehyde and semioxamazide lost the hydrazonic proton and coordinated to Ni(II) as tridentate via PNO atoms, with a cyanate anion occupying the fourth coordination place [4]. In square-planar Ni(II) complexes with the condensation derivative of 2-(diphenylphosphino)benzaldehyde and ethyl carbazate (**L1**) (ethyl (2*E*)-2-[2-(diphenylphosphino)benzylidene]hydrazinecarboxylate) the monoanionic ligand is coordinated

through the phosphorus, imine nitrogen and carbonyl oxygen atoms while the fourth coordination place is occupied with one of three different pseudohalides: cyanate, thiocyanate or azide [5]. Also, square-planar azido, isothiocyanato and cyanato Ni(II) complexes of 2-(diphenylphosphino)benzaldehyde 4-phenylsemicarbazone (**L2**) were reported [6]. As in the case of similar complexes with ethyl (2*E*)-2-[2-(diphenylphosphino)benzylidene] hydrazinecarboxylate the ligand was coordinated in deprotonated form via PNO donor atoms. It is interesting to note that until now there are no reported octahedral Ni(II) complexes of acylhydrazones of 2-(diphenylphosphino)benzaldehyde.

In this work, we report new insights from our continued interest on coordination properties of acylhydrazones of 2-(diphenylphosphino)benzaldehyde with ligand derived from Girard's T reagent and 2-(diphenylphosphino)benzaldehyde (**L3**) ((*E*)-2-(2-(2-(diphenylphosphino)-benzylidene)hydrazinyl)-*N*,*N*,*N*-trimethyl-2-oxoethan-1-aminium chloride) [7]. In particular, we focus here on its octahedral and square-planar isothiocyanato complexes of Ni(II). We report here synthesis, crystal structures, magnetic properties and DFT calculations for these compounds. Also, the influence of protonation of organic ligand on different stoichiometries and geometries observed for isothiocyanato complexes of Ni(II) with three different acylhydrazones of 2-(diphenylphosphino)benzaldehyde (**L1**, **L2** and **L3**) is explained on the basis of DFT calculations.

2. Experimental

2.1. Materials and techniques

2-(Diphenylphosphino)benzaldehyde (97%) and Girard's T reagent (99%) were obtained from Aldrich. The ligand was obtained by condensation reaction of 2-(diphenylphosphino)benzaldehyde and Girard's T reagent using a previously reported method [7]. IR spectra were recorded on a Perkin–Elmer FT-IR 1725X spectrometer using the ATR technique in the region 4000−400 cm^{-1} (vs-very strong, s-strong, m-medium, w-weak). Elemental analyses (C, H, and N) were performed by standard micro-methods using the ELEMENTARVario ELIII C.H.N.S.O analyzer. Molar conductivities were measured at room temperature (23 $^{\circ}$C) on a digital conductivity-meter JENWAY-4009. UV/Vis spectra were recorded at Shimadzu 1800 UV/Vis spectrometer. The temperature dependence of magnetic

susceptibility was studied on the powder sample by Quantum Design MPMS-XL-5 SQUID magnetometer in the temperature range 2–300 K, and under applied magnetic field of 1000 Oe.

2.2. Synthesis

*2.2.1. Synthesis of complex **1***

A mixture of 0.08 g (0.23 mmol) $Ni(BF_4)_2 \cdot 6H_2O$ and 0.11 g (0.23 mmol) of **L3** ligand was dissolved in 20 mL methanol and then 0.07 g (0.72 mmol) KSCN was added to it. The mixture was refluxed for 2 h and filtered. The reaction solution was cooled to room temperature and white precipitate (KBF_4) was filtered. Filtrate was left to stand at room temperature for three days while purple crystals arose from the solution. Yield 0.07 g (47%). IR: 3304 (w), 3017 (w), 2931 (w), 2764 (w), 2113 (s), 2067 (vs), 1659 (m), 1612 (m), 1475 (w),1435 (w), 1412 (w), 1333 (w), 1298 (w), 1089 (w), 976 (w), 918 (w), 794 (w), 755 (w), 696 (w). Elemental analysis calcd for $C_{27}H_{29}N_6NiO_2PS_3$: N 12.82 %, C 49.48 %, H 4.46 %, S 14.68 %, found: N 12.84 %, C 49.36 %, H 4.45 %, S 14.65 %. Λ_M (1 mM, DMSO): 12 Ω^{-1} cm^2 mol^{-1}. λ_{max} (nm) (H_2O): 277, 341, 363.

*2.2.2. Synthesis of complex **2***

A mixture of 0.08 g (0.23 mmol) $Ni(BF_4)_2 \cdot 6H_2O$ and 0.11 g (0.23 mmol) of **L3** ligand was dissolved in 20 mL methanol and then 0.06 g (0.79 mmol) NH_4SCN was added to it. The mixture was refluxed for 2 h. The reaction solution was left to stand at room temperature for two days while reddish crystals arose from the solution. Yield 0.09 g (64%). IR: 2071 (m), 1605 (w), 1568 (m), 1477 (w), 1432 (w), 1404 (w), 1343 (w), 1303 (w), 1035 (s), 973 (m), 910 (m), 871 (w), 845 (w), 810 (w), 771 (m), 749 (m), 691 (m), 665 (w). Elemental analysis calcd for $C_{25}H_{30}BF_4N_4NiO_3PS$: N 8.71 %, C 46.69 %, H 4.70 %, S 4.99 % found: N 8.79 %, C 46.35 %, H 4.74 %, S 5.05 %. Λ_M (1 mM, DMSO): 45.9 Ω^{-1} cm^2 mol^{-1}. λ_{max} (nm) (H_2O): 296, 327, 344, 362.

*2.2.3. Synthesis of complex **3***

In the mixture of 0.06 g (0.24 mmol) $Ni(AcO)_2 \cdot 4H_2O$ and 0.11 g (0.23 mmol) of **L3** ligand in 20 mL methanol 0.07 g (0.72 mmol) KSCN was added. The mixture was refluxed for 2 h. The reaction solution was left to stand at room temperature for two days while reddish crystals arose from the solution. Yield 0.10 g (73 %). IR: 3518 (w), 3382 (w), 3059 (w), 3017 (w), 2959 (w), 2080 (s), 2060 (s), 2005 (w), 1606 (w), 1571 (m), 1480 (m), 1433 (m), 1406 (w), 1344 (w), 1312 (w), 1101 (w), 998 (w), 978 (w), 935 (w), 914 (w), 750 (w), 692 (w). Elemental analysis calcd for $C_{26}H_{28}N_5NiO_2PS_2$: N 11.74 %, C 52.37 %, H 4.73 %, S 10.75 %, found: N 11.51 %, C 52.56 %, H 4.88 %, S 10.53 %. λ_M (1 mM, DMSO): 46.4 Ω^{-1} cm^2 mol^{-1}. λ_{max} (nm) (H_2O): 298, 328, 343, 362.

2.3. X-ray structure determinations

Crystal data and refinement parameters of compounds **1** and **2** are listed in Table 1. The X-ray intensity data were collected at room temperature with Agilent SuperNova dual source with an Atlas detector equipped with mirror-monochromated Mo Kα radiation (λ = 0.71073 Å). The data were processed using CRYSALIS PRO [8]. The structures were solved by direct methods (SIR-92 [9]) and refined by a full-matrix least-squares procedure based on F^2 using SHELXL-97 [10]. All non-hydrogen atoms were refined anisotropically. The N1 and C6 bonded hydrogen atoms in **1** and C6 bonded hydrogen atoms in **2** were located in a difference map and refined with the distance restraints (DFIX) with N-H = 0.86 and C-H = 0.98 and with U_{iso}(H) = 1.2U_{eq}(N) or U_{iso}(H) = 1.2U_{eq}(C), respectively. The water hydrogen atoms in **1** were also located in a difference map and refined with the distance restraints (DFIX) with O-H = 0.96 and with U_{iso}(O) = 1.5U_{eq}(O). All other hydrogen atoms were included in the model at geometrically calculated positions and refined using a riding model. It is also noteworthy that the thermal parameters of the S3 atom of one of the SCN^- ligands in **1** and F4 atom of BF_4^- ion in **2** are rather high. Spliting the location of these atoms in two different nearby positions using the PART instruction from the SHELXL routine result in a better agreement factor. Oxygen atoms belonging to water molecules in **2** exhibit large thermal ellipsoids due to the high mobility of the water molecules in the structures.

<**Table 1.**>

2.4. DFT computational details

The calculations using the unrestricted Kohn–Sham formalism have been performed with the Amsterdam Density Functional (ADF) program package, version 2013.01 [11] with generalized gradient approximation functional S12g which includes Grimme's D_3 dispersion energy [12]. Molecular orbitals were expanded in an uncontracted set of Slater type orbitals (STOs) [13], of triple-ζ quality containing diffuse functions plus one set of polarization functions (TZP). Small frozen core was used on all atoms because it was shown to have a negligible effect on the obtained geometries. Scalar relativistic corrections have been included self-consistently by using the zeroth-order regular approximation (ZORA). In order to check the possible influence of an environment, the calculations with a dielectric continuum model (COSMO) [14–16] (using methanol as a solvent) have been performed [17, 18]. Analytical harmonic frequencies were calculated and in all cases the global minimum was confirmed by the absence of imaginary frequency modes. In addition, for vacuo optimized geometries, thermochemical properties are derived at p = 1 atm and T = 298.15 K by using the standard statistical-mechanics relationships for an ideal gas.

3. Results and discussion

3.1. Synthesis

In the reaction of potentially tridentate (*E*)-2-(2-(2-(diphenylphosphino)-benzylidene)hydrazinyl)-*N*,*N*,*N*-trimethyl-2-oxoethan-1-aminium chloride monoethanole (**L3**) with $Ni(BF_4)_2{\cdot}6H_2O$ and KSCN in molar ratio 1 : 1 : 3 in methanol, the neutral octahedral complex **1** was obtained (Scheme 1). Precipitation of insoluble KBF_4 shifts the reaction equilibrium towards formation of complex **1**. In complex **1** the organic ligand is coordinated as tridentate through phosphorus, imine nitrogen and carbonyl oxygen atoms, while the remaining three coordination positions are occupied with *mer N*-coordinated thiocyanate anions. When the similar reaction was performed using NH_4SCN instead of KSCN as a source of thiocyanate anion the reaction product was square-planar complex **2** (Scheme 1). The cationic complex consisted of one molecule of deprotonated ligand coordinated in a tridentate PNO fashion to Ni(II) and a thiocyanate anion coordinated through nitrogen atom. Reaction of $Ni(AcO)_2{\cdot}4H_2O$, **L3** ligand and KSCN in molar ratio 1 : 1 : 3 in methanol resulted in the formation of a square-planar Ni(II)

complex **3** (Scheme 1). Complex **3** possesses the same cationic complex as complex **2** which is counterbalanced with a thiocyanate anion. In complexes **2** and **3**, deprotonation of the organic ligand results in the formation of formally neutral zwitter-ionic species. The positive charge of the quaternary ammonium group is compensated by the negative charge produced by the dissociation of the hydrazonic proton and the formation of a negatively charged oxygen atom after tautomerization. Previously reported isothiocyanato complexes of Ni(II) with ethyl (2*E*)-2-[2-(diphenylphosphino)benzylidene]hydrazinecarboxylate (**L1**) [5] and 2-(diphenylphosphino)benzaldehyde 4-phenylsemicarbazone (**L2**) [6] were obtained in the reaction of the corresponding ligand, $Ni(AcO)_2 \cdot 4H_2O$ and NH_4SCN, while in the reaction of these ligands with $Ni(BF_4)_2 \cdot 6H_2O$ and KSCN it was not possible to obtain stable octahedral complex (Scheme 2).

<Scheme 1.>

<Scheme 2.>

3.2. Spectroscopy

Different coordination modes of thiocyanato anions in complexes **1**, **2** and **3** can be deduced on the basis of the position and number of bands in the *ν*(CN) vibration range of the NCS^- group in IR spectra. The presence of two bands in the *ν*(CN) vibration range of NCS^- group in the spectrum of **1** confirms the coordination of isothiocyanato ligands in apical (2113 cm^{-1}) and equatorial (2067 cm^{-1}) position. In the IR spectrum of **2** a band at 2071 cm^{-1} corresponds to only one NCS group coordinated to Ni(II) via the nitrogen atom, while in the spectrum of complex **3** two strong *ν*(CN) bands at 2080 cm^{-1} and 2060 cm^{-1} originating from NCS groups are presented. The band at higher energy belongs to the NCS group coordinated through the nitrogen atom, while the lower energy band corresponds to a non-coordinated thiocyanate anion [19]. The presence of a non-coordinated thiocyanate anion in complex **3** is also confirmed on the basis of the result of molar conductivity measurements. Coordination of the imine nitrogen in complexes **1**, **2** and **3** was confirmed on the basis of the bathochromical shift of the *ν*(C=N) vibration from 1657 cm^{-1} in the spectra of the ligand to 1612 cm^{-1} in the spectrum of

1, 1605 cm^{-1} in the spectrum of **2** and 1606 cm^{-1} in the spectrum of **3**. Coordination of the deprotonated ligand in complexes **2** and **3** is shown through the appearance of a new band corresponding to $\nu(^{-}O–C=N)$ of the deprotonated hydrazide moiety at 1568 cm^{-1} in the spectrum of **2** and 1571 cm^{-1} in the spectrum of **3**, instead of the carbonyl band from the uncoordinated ligand at 1686 cm^{-1}. The negative shift of the ν(C=O) vibration which is in the spectrum of complex **1** observed at 1659 cm^{-1} was related to the coordination of the oxygen atom of the carbonyl group. The position of the band assigned to ν(C–P) vibrations is almost constant in the IR spectra of ligand and the complexes (1433 cm^{-1} in the spectrum of ligand, 1435 cm^{-1} in the spectrum of complex **1**, 1432 cm^{-1} in the spectrum of complex **2** and 1433 cm^{-1} in the spectrum of complex **3**). In the IR spectrum of complex **2** a band at 1035 cm^{-1} originates from the tetrafluoroborate anion in the outer sphere of the complex.

Electronic spectra of complexes **1**, **2** and **3** are similar, without electronic transitions below 10000 cm^{-1} indicating square-planar geometry of complexes in solution [20]. Octahedral complex **1** is unstable in solution; apical isothiocyanato ligands readily dissociate from metal ion. Final confirmation of the structures of complex **1** and **2** in solid state was given by X-ray analysis.

3.3. Description of the crystal structures

Crystals of products **1** and **2** suitable for X-ray analyses were prepared by slow evaporation of solvent at room temperature. Selected bond lengths and angles are given in Table 2. The structure of complex **1** possesses the tridentate **L3** ligand and complex **2** deprotonated tridentate **L3** ligand, both coordinated to the nickel atom with a PNO set of donor atoms forming one five-membered and one six-membered chelate ring.

The structure of compound **1** is displayed in Figure 1. The three thiocyanate nitrogen atoms complete the distorted octahedral coordination mode of nickel atom in complex **1**. Intermolecular interactions that exist in the solid state of compounds **1** are depicted in Fig. 2. N-H···O and O-H···S hydrogen bonds connect the complex molecules and water molecules into an infinite chain. Hydrogen-bonding interactions for compound **1** are listed in Table 3.

The cationic complex in **2** consists of one tridentate molecule of deprotonated **L3** ligand coordinated to the Ni(II) ion and thiocyanate anion coordinated through nitrogen atom forming a

square planar geometry around the Ni(II) ion. The BF_4^- ion acts as counter-ion in the crystal structure. There are also two water molecules as solvent per one ionic formula unit. The sum of the nickel-containing angles in complexes **2** is 360°. The position of the Ni(II) ion is 0.063(14) out of the best plane that contained the coordination sphere of four atoms. The observed elongation of O1–C5 and shortening of N1–C5 bond in complex **2** in comparison with the corresponding bonds in complex **1** (Table 2) indicates electron delocalization in the deprotonated hydrazine moiety and coordination of the ligand in enol form. In the structure of complex **2** there is no evidence for any significant non-covalent interactions.

<**Fig. 1.**>

<**Fig. 2.**>

<**Fig. 3.**>

<**Table 2.**>

<**Table 3.**>

3.4. Magnetic measurements

The data were corrected for the contributions of the sample holder and for the diamagnetism of the sample estimated from Pascal's constants. Magnetic data for complex **1** are shown in Fig. 4, where temperature dependence of inverse magnetic susceptibility ($1/\chi$) and effective magnetic moment (μ_{eff}), per mol of Ni(II) complex are presented. It can be seen linear behavior of inverse magnetic susceptibility in the whole temperature range showing

paramagnetic behavior of the investigated sample. Fitting the susceptibility data to the Curie–Weiss law $\chi = C/(T-\theta)$ (where C and θ present Curie constant and Weiss temperature, respectively), gave $C = 1.20$ cm^{3}mol^{-1}K^{-1}, and $\theta = -0.1$ K. The effective magnetic moment μ_{eff} = 3.1 μ_B, obtained from Curie constant C, is slightly higher than the spin-only value for Ni^{2+} ion (μ_{eff} = 2.82 μ_B), but it is in a good agreement with literature data for Ni^{2+} in octahedral environment [22, 23]. Small negative value obtained for Weiss constant is within the experimental error. Curve $\mu_{eff}(T)$ shows that magnetic moment is almost constant, starting from room temperature (3.12 μ_B) to 8 K, and for lower temperature (T = 2 K) slightly decreases to 2.85 μ_B, which is only 9% of the nominal value at 293 K.

<Fig. 4.>

3.5. DFT calculations

Depending on the side chain of the 2-(diphenylphosphino)benzaldehyde core and source of Ni^{2+} and SCN^- ions isothiocyanato Ni(II) complexes of different geometry and stoichiometry were obtained. Among the investigated acylhydrazones of 2-(diphenylphosphino)benzaldehyde only (*E*)-2-(2-(2-(diphenylphosphino)benzylidene)hydrazinyl)-*N*,*N*,*N*-trimethyl-2-oxoethan-1-aminium chloride (**L3**) ligand formed both the octahedral and square planar Ni(II) complexes, while with the other examined ligands, i.e. ethyl (2*E*)-2-[2-(diphenylphosphino)benzylidene] hydrazinecarboxylate (**L1**) and 2-(diphenylphosphino)benzaldehyde 4-phenylsemicarbazone (**L2**) the square planar geometry have been obtained, Scheme 1 and Scheme 2. Bearing in the mind that the octahedral complex is isolated with the protonated form of the ligand, and square-planar complexes are isolated with deprotonated forms, we performed density functional theory (DFT) calculations in order to estimate the relative energetics of reactions (with both protonated and deprotonated forms of the ligands). Also, the ligand field splitting analysis has been done to gain deeper insight into the relationship between the geometrical structure of the isolated complex and the protonation of the ligand.

The reaction that converts the deprotonated square-planar complexes to protonated octahedral complexes was not under study since it would include the absolute free energy of a proton, Scheme 3a. Instead, we computationally examined reactions with only protonated or

deprotonated form of the ligand, Scheme 3b, in the gas phase as well as in methanol solution. It is worth noting that an evaluation of the entropies (and so the Gibbs free energies) of the chemical reactions in solution is a challenge for computational chemists. The contributions for S_{trans} and S_{rot} in COSMO are calculated for the molecule in the gas phase, and translational entropy is obviously reduced in fluid [24–26]. As a result, the Gibbs free energies in COSMO environment are excluded from the discussion even though they do not deviate from the observed trends.

<Scheme 3.>

Computed thermochemical properties, on optimized geometries in the gas phase, for the reactions in Scheme 3b, are given in Table 4. The trends in electronic energies, reaction enthalpies and Gibbs free energies calculated in the gas phase are completely the same, and they clearly indicate that the formation of the protonated octahedron, in all cases, is much more favorable than the deprotonated one. The reaction energies in the gas phase are of course largely influenced by the overall charge of the complex, which leads to large solvent effects (*vide infra*). Furthermore, within the series of protonated octahedral structures, the most favorable one is the formation of the experimentally obtained structure.

The influence of the solvent environment is clearly visible when we look at single point COSMO calculations on the gas-phase optimized geometries. Because of the overall charge of the complex, leading to large solvation energies, the COSMO reaction energies are in absolute sense drastically different from the gas-phase values. Regardless of this quantitative difference, all the above trends are still valid. To make sure that the solvent does not have a significant effect on the trends through drastic changes in the structures, we repeated all optimizations including the COSMO solvent environment explicitly. These results are in very good agreement with the single-point COSMO results on the gas-phase geometries (see Table S2). One of the key points in understanding the preference for either square-planar or octahedral coordination is therefore the overall charge of the ligand (and hence the complex). Overall, the calculated reaction energies indicate that the most favorable energy of formation corresponds to the experimentally obtained octahedron.

<**Table 4.**>

The results of the analysis of the ligand field splitting in complexes with protonated and deprotonated forms of ligands are quite straightforward. The deprotonated form of the ligand produces a stronger orbital splitting both in square-planar and in octahedral environment, see Scheme 4.

This follows the experimental results very well, since the low spin square-planar structures that require the stronger ligand field to be formed are isolated only with the deprotonated ligand, while the high spin octahedral structure is found with the protonated form. It is now clear why the reaction energetics for the protonated square-planar/octahedral pair is always more negative than with the deprotonated one (electronic factors favour the product in the first and reactant in the second case).

<Scheme 4.>

Selected bond lengths of the gas-phase and COSMO optimized structures, reaction energies for the COSMO optimized geometries, and Cartesian coordinates are given in the Supplementary Information.

Furthermore, within the series of protonated octahedral structures, the most favorable one is the formation of the experimentally obtained structure.

Having in mind trends in calculated electronic energies, reaction enthalpies and Gibbs free energies as well as the results of the analysis of the ligand field splitting it is clear that the formation of high spin octahedral structure is favored with protonated form of ligand.

Conclusion

In this paper we describe the synthesis and characterization of three Ni(II) isothiocyanato complexes with (*E*)-2-(2-(2-(diphenylphosphino)benzylidene)hydrazinyl)-*N*,*N*,*N*-trimethyl-2-

oxoethan-1-aminium chloride. Depending on the reaction conditions, i.e. the source of Ni^{2+} and SCN^- ions, complexes with different stoichiometry's and geometries were obtained. Coordination of the deprotonated phosphine ligand results in formation of square-planar complexes, while the octahedral complex was formed with the protonated ligand. In the reaction of **L3** ligand with $Ni(BF_4)_2 \cdot 6H_2O$ and KSCN in methanol precipitation of insoluble KBF_4 favored the reaction equilibrium towards formation of octahedral complex. Also, formation of an infinite chain of complex and water molecules connected by hydrogen bonds stabilizes octahedral structure of compound **1** in solid state. In all the complexes one molecule of organic ligand was coordinated in PNO fashion and the remaining coordination positions were occupied with thiocyanate ions.

Magnetic data were analyzed by Curie-Weiss law from where effective magnetic moment (μ_{eff}=3.1μ_B) for Ni^{2+} was obtained. $1/\chi$(T) and μ_{eff}(T) curves show paramagnetic behavior of investigated Ni(II) complex **1**.

Reaction energetics and ligand field splittings of Ni(II) complexes with three different 2-(diphenylphosphino)benzaldehyde acylhydrazone were studied by means of density functional theory, since the octahedral coordination geometry was obtained experimentally only with (*E*)-2-(2-(2-(diphenylphosphino)benzylidene)hydrazinyl)-*N*,*N*,*N*-trimethyl-2-oxoethan-1-aminium chloride monoethanole.

The trends in calculated electronic energies, reaction enthalpies and Gibbs free energies indicate that the formation of the protonated octahedron, in all cases, is much more favorable than the deprotonated one.

The results of the analysis of the ligand field splitting in complexes with protonated and deprotonated forms of ligands shows that the deprotonated form of the ligand produces a stronger orbital splitting both in square-planar and in octahedral environment.

This is in accordance with the experimental results, since the low spin square-planar structures that require the stronger ligand field are isolated only with the deprotonated ligand, while the high spin octahedral structure is found with the protonated form.

Acknowledgments

This work was supported by the Ministry of Education, Science and Technological development of the Republic of Serbia (Grant OI 172055). We thank the Slovenian Research Agency (ARRS) through program P-0175 for financial support and EN-FIST Centre of Excellence, Dunajska 156, 1000 Ljubljana, Slovenia, for using SuperNova diffractometer. The following organizations are thanked for financial support: the Ministerio de Ciencia e Innovación (MICINN, project number CTQ2011-25086/BQU), and the DIUE of the Generalitat de Catalunya (project number 2014SGR1202 and the XRQTC). Financial support from MICINN (Ministry of Science and Innovation, Spain) and the FEDER fund (European Fund for Regional Development) was provided by grant UNGI08-4E-003. Excellent service by the Centre de Serveis Científics i Acadèmics de Catalunya (CESCA) is gratefully acknowledged. Part of this work was supported by COST Action CM1305 ‘‘Explicit Control Over Spin-states in Technology and Biochemistry (ECOSTBio)’’.

Appendix A. Supplementary data

CCDC 1033152–1033153 contains the supplementary crystallographic data for **1** and **2**, respectively. These data can be obtained free of charge from The Cambridge Crystallographic Data Centre *via* www.ccdc.cam.ac.uk/data_request/cif.

References

[1] (a) A. Bacchi, M. Carcelli, M. Costa, A. Leporati, E. Leporati, P. Pelagatti, C. Pelizzi, G. Pelizzi, J. Organomet. Chem. 535 (1997) 107–120. (b) P. Pelagatti, A. Bacchi, M. Carcelli, M. Costa, A. Fochi, P. Ghidini, E. Leporati, M. Masi, C. Pelizzi, G. Pelizzi, J. Organomet. Chem. 583 (1999) 94–105. (c) P. Pelagatti, A. Bacchi, C. Bobbio, M. Carcelli, M. Costa, C. Pelizzi, C. Vivorio, Organometallics 19 (2000) 5440–5446. (d) P. Pelagatti, A. Bacchi, C. Bobbio, M. Carcelli, M. Costa, A. Fochi, C. Pelizzi, J. Chem. Soc., Dalton Trans. (2002) 1820–1825. (e) P. Pelagatti, A. Bacchi, M. Carcelli, M. Costa, H. Frühauf, K. Goubitz, C. Pelizzi, M. Triclistri, K. Vrieze, Eur. J. Inorg. Chem. (2002) 439–446. (f) P. Pelagatti, A. Bacchi, M. Balordi, S. Bolaño, F. Calbiani, L. Elviri, L. Gonsalvi, C. Pelizzi, M. Peruzzini, D. Rogolino, Eur. J. Inorg. Chem. (2006) 2422–2436. (g) P. Pelagatti, A. Bacchi, M. Balordi, A. Caneschi, M. Giannetto, C. Pelizzi, L. Gonsalvi, M. Peruzzini, F. Ugozzoli, Eur. J. Inorg. Chem. (2007) 162–171. (h) M.M. Đorđević, D.A. Jeremić, M.V. Rodić, V.S. Simić, I.D. Brčeski, V.M. Leovac, Polyhedron 68 (2013) 234–240. (i) M. Milenković, A. Bacchi, G. Cantoni, S. Radulović, N. Gligorijević, S. Aranđelović, D. Sladić, M. Vujčić, D. Mitić, K. Anđelković, Inorg. Chim. Acta 395 (2013) 33–43. (j) M. Milenković, G. Cantoni, A. Bacchi, V. Spasojević, M. Milenković D. Sladić, N. Krstić, K. Anđelković, Polyhedron, 80 (2014) 47–52.

[2] A. Bacchi, M. Carcelli, M. Costa, A. Fochi, C. Monici, P. Pelagatti, C. Pelizzi, G. Pelizzi, L.M.S. Roca, J. Organomet. Chem. 593–594 (2000) 180–191.

[3] S.B. Novaković, G.A. Bogdanović, I.D. Brčeski, V.M. Leovac, Acta Crystallogr C. 65 (2009) 263–265.

[4] V. Radulović, A. Bacchi, G. Pelizzi, D. Sladić, I. Brčeski, K. Andjelković, Monatsh. Chem. 137 (2006) 681–691.

[5] M. Milenković, A. Bacchi, G. Cantoni, J. Vilipić, D. Sladić, M. Vujčić, N. Gligorijević, K. Jovanović, S. Radulović, K. Anđelković, Eur. J. Med. Chem. 68 (2013) 111–120.

[6] M. Milenković, A. Pevec, I. Turel, M. Vujčić, M. Milenković, K. Jovanović, N. Gligorijević, S. Radulović, M. Swart, M. Gruden-Pavlović, K. Adaila, B. Čobeljić, K. Anđelković, Eur. J. Med. Chem. 87 (2014) 284–297.

[7] K. Adaila, M. Milenković, A. Bacchi, G. Cantoni, M. Swart, M. Gruden-Pavlović, M. Milenković, B. Čobeljić, T. Todorović, K. Anđelković, J.Coord.Chem. 67 (2014) 3633–3648.

[8] Oxford Diffraction, CrysAlis PRO, Oxford Diffraction Ltd., Yarnton, England, 2009.

[9] A. Altomare, G. Cascarano, C. Giacovazzo, A. Guagliardi, J. Appl. Crystallogr. 26 (1993) 343–350.

[10] G.M. Sheldrick, Acta Crystallogr. A, 64 (2008) 112–122.

[11] E.J. Baerends, J. Autschbach, A. Bérces, J.A. Berger, F.M. Bickelhaupt, C. Bo, P.L. de Boeij, P.M. Boerrigter, L. Cavallo, D.P. Chong, L. Deng, R.M. Dickson, D.E. Ellis, M. van Faassen, L. Fan, T.H. Fischer, C.F. Guerra, S.J.A. van Gisbergen, J.A. Groeneveld, O.V. Gritsenko, M. Grüning, F.E. Harris, P. van den Hoek, C.R. Jacob, H. Jacobsen, L. Jensen, E.S. Kadantsev, G. van Kessel, R. Klooster, F. Kootstra, E. van Lenthe, D.A. McCormack, A. Michalak, J. Neugebauer, V.P. Nicu, V.P. Osinga, S. Patchkovskii, P.H.T. Philipsen, D. Post, C.C. Pye, W. Ravenek, P. Romaniello, P. Ros, P. R. T. Schipper, G. Schreckenbach, J.G. Snijders, M. Solà, M. Swart, D. Swerhone, G. teVelde, P. Vernooijs, L. Versluis, L. Visscher, O. Visser, F. Wang, T.A. Wesolowski, E.M. van Wezenbeek, G. Wiesenekker, S.K. Wolff, T.K. Woo, A.L. Yakovlev, T. Ziegler, SCM, Amsterdam, 2013.01 edn., 2013, p. ADF.

[12] M. Swart, Chem. Phys. Lett. 580 (2013) 166–171.

[13] E. van Lenthe, E.J. Baerends, J. Comput. Chem. 24 (2003) 1142–1156.

[14] A. Klamt, G. Schüürmann, J. Chem. Soc. Perkin Trans.2 (1993) 799–805.

[15] A. Klamt, V. Jones, J. Chem. Phys. 105 (1996) 9972–9981.

[16] A. Klamt, J. Phys. Chem. 99 (1995) 2224–2235.

[17] C.C. Pye, T. Ziegler, Theor. Chem. Acc. 101 (1999) 396–408.

[18] M. Swart, E. Rösler, F.M. Bickelhaupt, Eur. J. Inorg. Chem. (2007) 3646–3654.

[19] K. Nakamoto, Infrared and Raman Spectra of Inorganic and Coordination Compounds, fourth ed.,Wiley-Interscience, New York, 2009.

[20] A.B.P. Lever, in: M.F. Lappert (Ed.), Physical Inorganic Chemistry, Elsevier, Amsterdam, 1968.

[21] K. Brandenburg, DIAMOND, Crystal and Molecular Structure Visualization Version 3.2, Crystal Impact GbR, Bonn, Germany.

[22] B. Čobeljić, B. Warżajtis, U. Rychlewska, D. Radanović, V. Spasojević, D. Sladić, R. Eshkourfu, K. Anđelković, J.Coord.Chem. 65 (2012) 655–667.

[23] S. Wöhlert, T. Runčevski, R.E. Dinnebier, S.G. Ebbinghaus, C. Näther, Cryst.Growth Des. 14 (2014) 1902–1913.

[24] C. Spickermann, T. Felder, C.A. Schalley, B. Kirchner, Chem. Eur. J. 14 (2008) 1216–1227.

[25] M. Garcia-Borràs, J.M. Luis, M. Swart, M. Solà, Chem. Eur. J. 19 (2013) 4468–4479.

[26] Z.-X. Yu, K.N. Houk, J. Am. Chem. Soc. 125 (2003) 13825–13830.

Scheme caption:

Scheme 1. Synthesis of Ni(II) isothiocyanato complexes with (*E*)-2-(2-(2-(diphenylphosphino) benzylidene)hydrazinyl)-*N*,*N*,*N*-trimethyl-2-oxoethan-1-aminium chloride (**L3**).

Scheme 2. Synthesis of Ni(II) isothiocyanato complexes with ethyl (2*E*)-2-[2-(diphenylphosphino)benzylidene]hydrazinecarboxylate (**L1**) and 2-(diphenylphosphino)benzaldehyde 4-phenylsemicarbazone (**L2**).

Scheme 3. Formation of octahedral coordination geometries: a) transformation of deprotonated Ni(II) complex into protonated octahedron; b) transformation of square-planar complexes into octahedrons, separately with protonated and deprotonated forms of ligand.

Scheme 4. *d*-orbital splitting for the investigated complexes.

Figure caption:

Fig. 1. ORTEP plot of **1** with thermal ellipsoids at 30% probability for non-H atoms and open circles for H-atoms.

Fig. 2. DIAMOND [21] view of **1** showing the polymeric chain in the crystal structure [Symmetry code: (i) x, –y+1/2, z–1/2].

Fig. 3. ORTEP plot of **2** with thermal ellipsoids at 30% probability for non-H atoms and open circles for H-atoms. BF_4^- and two water molecules were omitted for clarity reasons.

Fig. 4. Temperature dependences of inverse magnetic susceptibility (open circles) and effective magnetic moment (open squares). Solid line is fit to Curie–Weiss law.

Table caption:

Table 1. Crystal data and structure refinement details for **1** and **2**.

Table 2. Selected bond lengths (Å) and angles (°) of compounds **1** and **2**.

Table 3. Hydrogen bonding geometry for **1**.

Table 4. Energy difference between the product and the sum of the reactants from Scheme 3b.

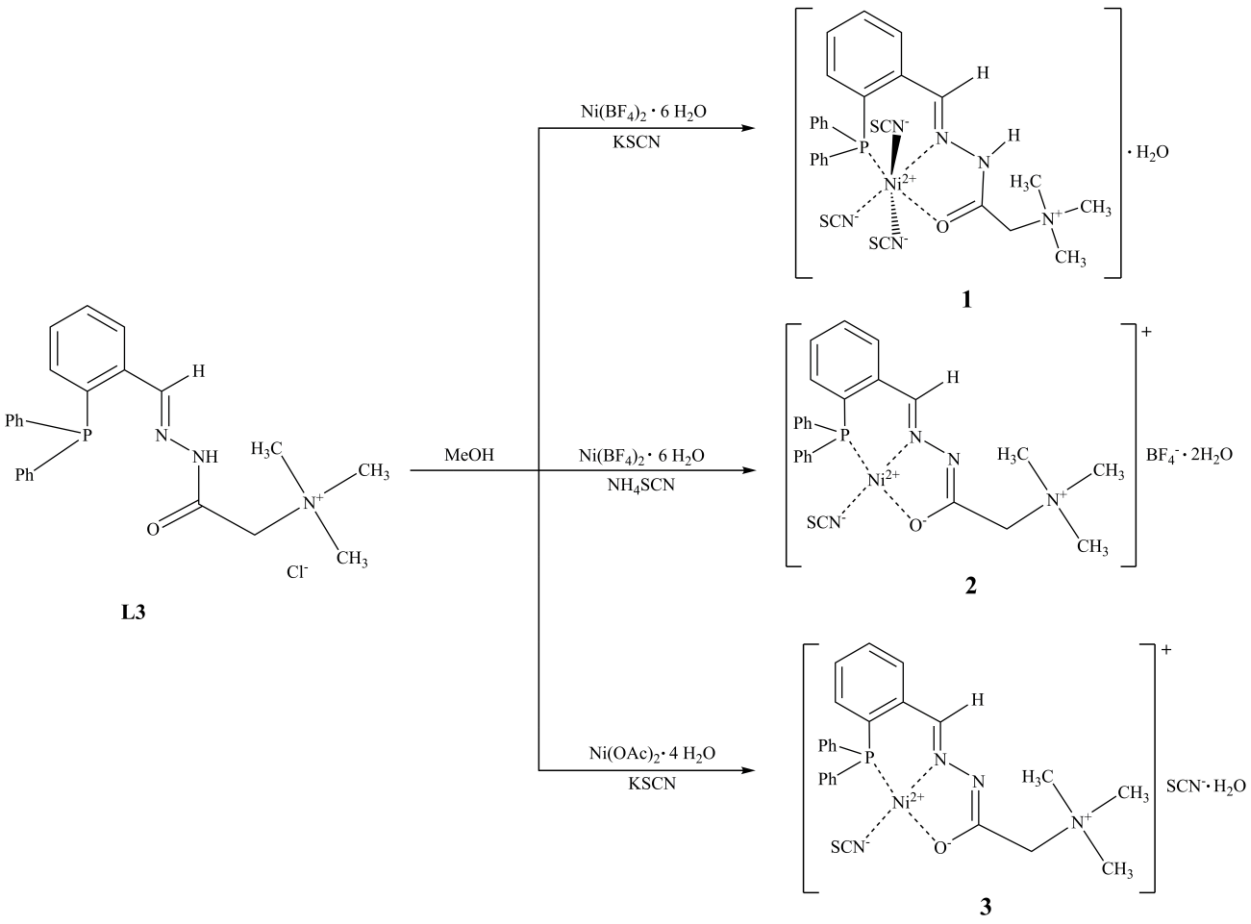

Scheme 1.

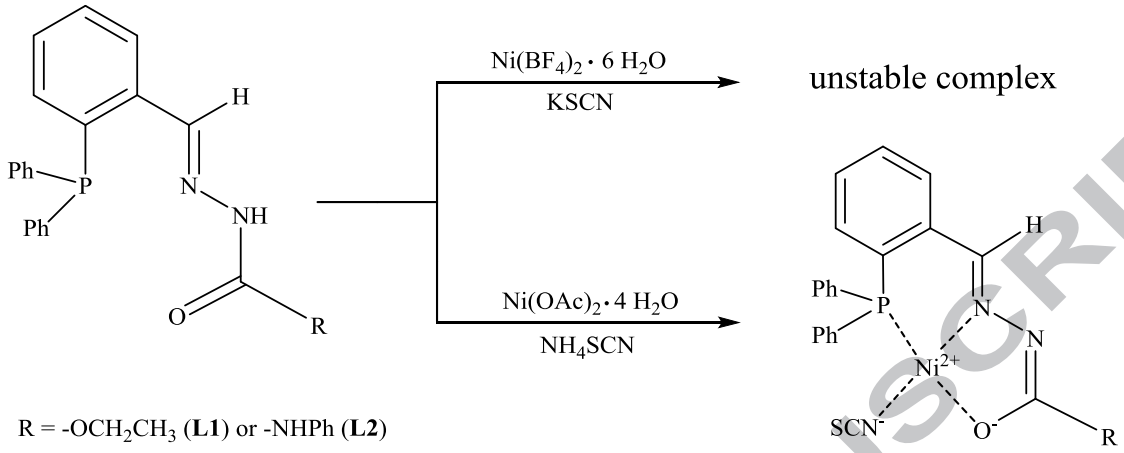

R = -OCH_2CH_3 (**L1**) or -NHPh (**L2**)

Scheme 2.

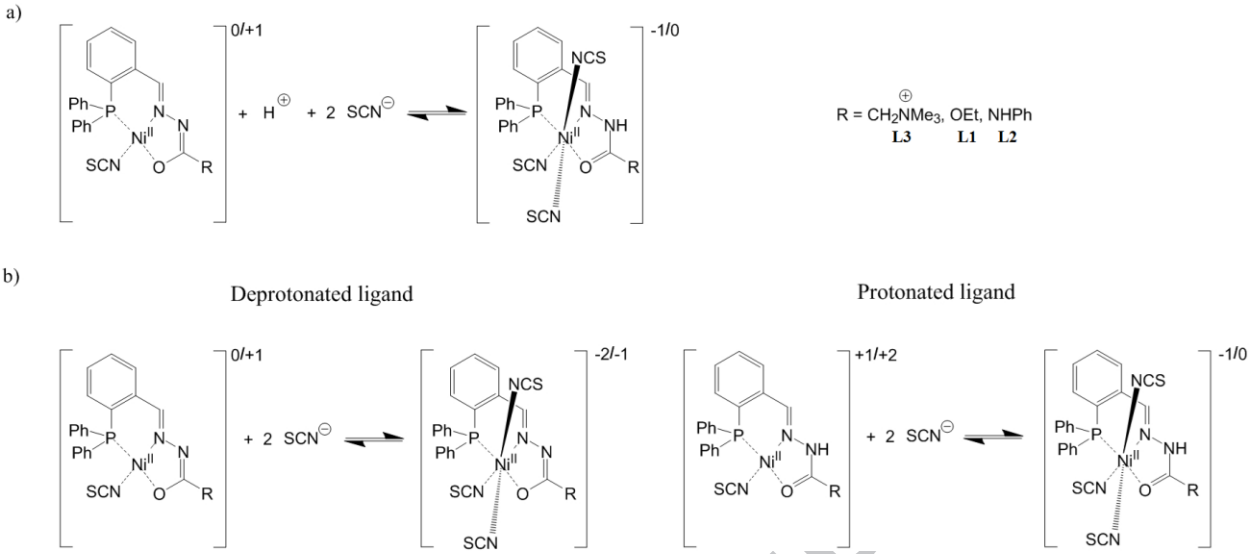

Scheme 3.

Orbital splitting in eV

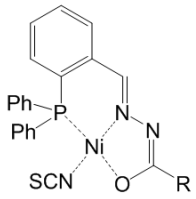

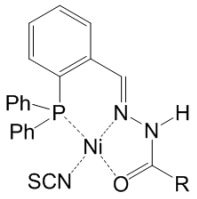

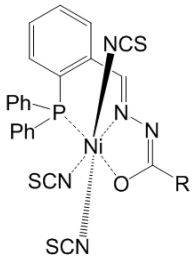

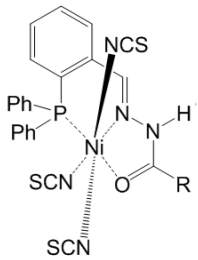

R = CH_2NMe_3 (**L3**)	2.758	2.319	1.509	1.314
R = OEt (**L1**)	2.757	2.310	1.492	1.345
R = NHPh (**L2**)	2.756	2.244	1.468	1.342

Scheme 4.

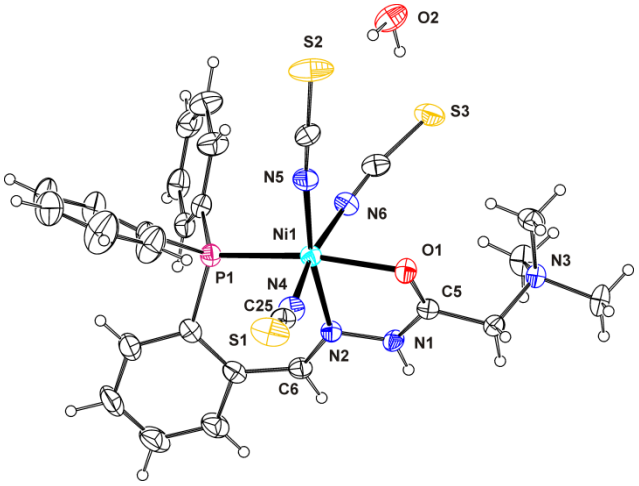

Figure 1.

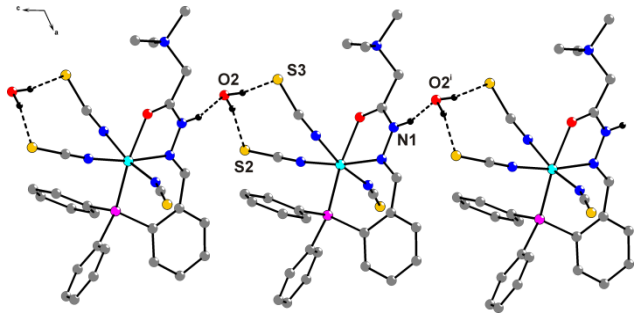

Figure 2.

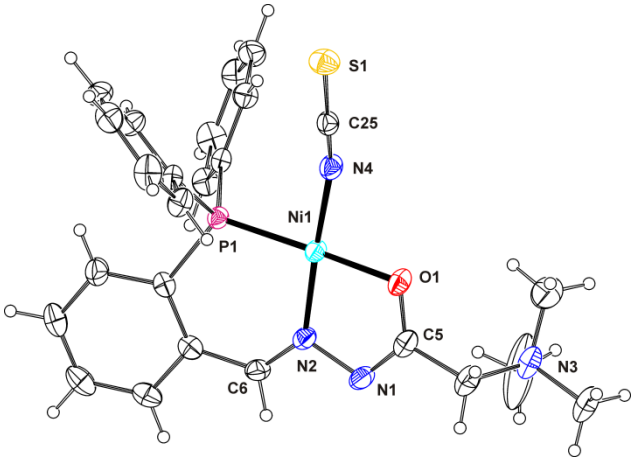

Figure 3.

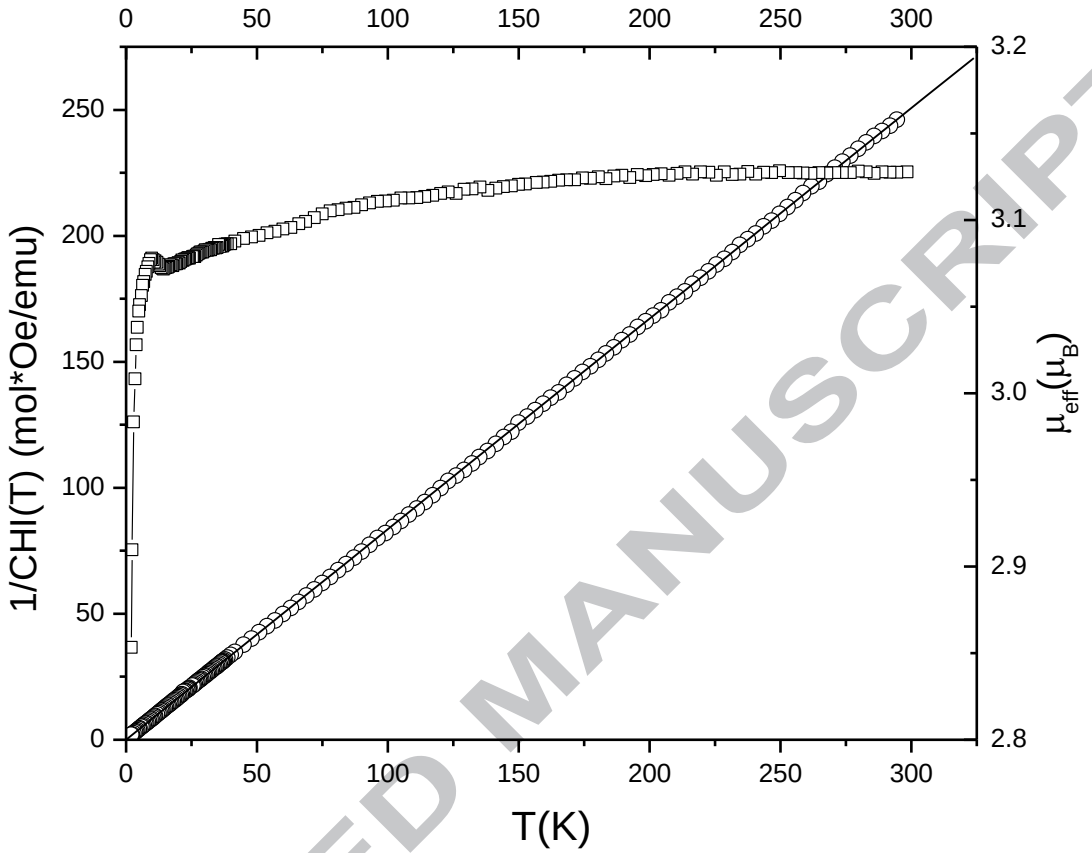

Figure 4.

Table 1. Crystal data and structure refinement details for **1** and **2**.

	1	**2**
formula	$C_{27}H_{29}N_6NiO_2PS_3$	$C_{25}H_{30}BF_4N_4NiO_3PS$
Fw (g mol^{-1})	655.42	643.08
crystal size (mm)	0.10 × 0.05 × 0.05	0.50 × 0.05 × 0.05
crystal color	purple	red
crystal system	monoclinic	monoclinic
space group	$P2_1/c$	$P2_1/c$
a (Å)	19.394(2)	13.7978(4)
b (Å)	10.4468(4)	11.5110(3)
c (Å)	17.1915(12)	17.7664(6)
β (º)	116.060(10)	93.241(3)
V (Å^3)	3128.9(4)	2817.26(15)
Z	4	4
calcd density (g cm^{-3})	1.391	1.516
F(000)	1360	1328
no. of collected reflns	11019	13264
no. of independent reflns	6303	6441
R_{int}	0.0447	0.0376
no. of reflns observed	3733	4389
no. parameters	386	377
$R[I > 2\sigma(I)]^a$	0.0527	0.0586
wR_2 (all data)^b	0.1028	0.1616
Goof , S^c	1.007	1.031
maximum/minimum residual electron density (e Å^{-3})	+0.31/–0.35	+0.69 /–0.62

^{a} $R = \sum||F_o| - |F_c||/\sum|F_o|$. ^{b} $wR_2 = \{\sum[w(F_o^2 - F_c^2)^2]/\sum[w(F_o^2)^2]\}^{1/2}$.
^{c} $S = \{\sum[w(F_o^2 - F_c^2)^2]/(n/p\}^{1/2}$ where n is the number of reflections and p is the total

Table 2. Selected bond lengths (Å) and angles (°) of compounds **1** and **2**.

	1	**2**
Ni1–P1	2.3724(10)	2.1469(10)
Ni1–O1	2.153(2)	1.903(3)
Ni1–N2	2.087(3)	1.863(3)
Ni1–N4	2.035(3)	1.859(3)
Ni1–N5	2.010(3)	–
Ni1–N6	2.099(3)	–
N1–N2	1.385(3)	1.415(4)
N1–C5	1.345(4)	1.291(5)
N2–C6	1.288(4)	1.280(5)
O1–C5	1.229(3)	1.290(5)
S1–C25	1.631(4)	1.616(4)
C25–N4	1.150(4)	1.159(5)
P1–Ni1–O1	166.64(6)	175.81(9)
P1–Ni1–N4	95.96(9)	88.63(10)
P1–Ni1–N5	98.35(9)	–
P1–Ni1–N6	93.64(9)	–
N2–Ni1–N4	92.11(11)	174.59(14)
N1–N2–C6	115.0(3)	112.8(3)
N1–C5–O1	121.7(3)	126.0(4)
N2–N1–C5	118.2(3)	109.2(3)

Table 3. Hydrogen bonding geometry for **1**.

D – H ⋯ A	*d*(D – H)/ Å	*d*(H ⋯ A)/ Å	*d*(D ⋯ A)/ Å	<(DHA)/ º	Symmetry transformation for acceptors
N1–H1N···O2	0.841(17)	1.94(2)	2.744(4)	159(3)	x, –y+1/2, z–1/2
O2–H1···S2	0.954(19)	2.28(2)	3.218(3)	168(4)	
O2–H2···S3	0.947(19)	2.37(2)	3.295(11)	165(4)	

Table 4. Energy difference between the product and the sum of the reactants from Scheme 3b.

Side chain R	$\Delta E_{vac.}$	$\Delta H_{vac.}$	$\Delta G_{vac.}$ [a]	$\Delta E_{sp/cosmo}$ [b]
deprotonated ligand				
R= $-CH_2N^{(+)}(CH_3)_3$	–100.75	–100.50	–79.03	–7.04
R= -OEt	12.16	12.15	33.21	–3.64
R= -NHPh	9.83	9.07	31.77	–3.92
protonated ligand				
R= $-CH_2N^{(+)}(CH_3)_3$	–239.30	–237.95	–215.23	–25.13
R= -OEt	–116.83	–116.75	–93.34	–16.24
R= -NHPh	–116.42	–116.45	–92.75	–9.64

a) calculated at p=1 atm and T=298.15 K; b) single point calculations with COSMO on gas-phase optimized geometries

Synthesis and characterization of octahedral and square-planar isothiocyanato Ni(II) complexes with acylhydrazones of 2-(diphenylphosphino)benzaldehyde. DFT explanation of the influence of phosphine ligand protonation on geometry and stochiometry of complexes. Magnetic properties of octahedral Ni(II) complex.